COMPDYN 2015
5th ECCOMAS Thematic Conference on
Computational Methods in Structural Dynamics and Earthquake Engineering
M. Papadrakakis, V. Papadopoulos, V. Plevris (eds.)
Crete Island, Greece, 25–27 May 2015

PERFORMANCE OF STEEL COLUMNS SUBJECTED TO VEHICLE IMPACT – EXPERIMENTAL AND NUMERICAL STUDIES

J. Korndörfer, B. Hoffmeister and M. Feldmann

Institute for Steel Structures, RWTH Aachen
Mies-van-der-Rohe-Str. 1, 52074 Aachen, Germany
e-mail: korndoerfer@stb.rwth-aachen.de

Keywords: Impact tests, steel columns, member-structure interaction, LS-Dyna.

Abstract. *Hazard scenarios regarding exceptional actions often include the possibility of a vehicle impact against a building. Here the impact against columns is of particular interest as they are the most exposed members. At the same time consequences are vast, since their failure can result in the collapse of the building.*

To evaluate the dynamic response of an impacted member, six slightly downscaled vehicle impact tests have been performed at RWTH Aachen University. Three different boundary conditions for the column have been examined, including a simply supported column (ideally pinned) with and without a concentrated mass attached to the column head as well as a column with realistic boundary conditions and connections at column base and column head. By varying the boundary conditions and the attached mass the influence of various types of interaction between the column and the surrounding structure has been assessed experimentally. Also the velocity of the impact body has been varied to achieve different degrees of impairment and residual strengths of the column.

In a second step state of the art commercial software (LS-Dyna) has been used to perform impact simulations with refined finite element models to augment the experimental results. Different member configurations have been investigated to further evaluate the influence of several parameters like impact velocity, mass and stiffness distribution of the member. The numerical models together with the implemented fundamental physical laws were validated by recalculations of the experimental tests.

1 INTRODUCTION

The European project 'Robustimpact' aims at the development of an innovative design concept that helps to properly assess and improve the resistance of steel structures subjected to impact loads. One of the design concepts followed within this project is the residual strength method which aims for high energy dissipation through plastic deformation of the impacted member, exploiting the extremely ductile behaviour of steel, while keeping sufficient residual strength for global structural stability after the impact.

The level of residual strength of an impacted steel column highly depends on the deformation caused by the impact since lateral deflections of the member imply additional bending moments due to axial loading. Steel columns are typically characterised by a high slenderness ratio which means that not only bending, but also stability failure must be considered as a possible ultimate limit state. In general, the level of deformation caused by impact loading cannot be assessed properly without taking the correct boundary conditions as well as the stiffness and mass of the surrounding structure into account. Earlier studies [1] have shown, that the inertia of the connected mass is able to provide significant axial restraint during the first phase of the impact, resulting in reduced deflections at the point of impact.

2 EXPERIMENTAL INVESTIGATIONS

To investigate the response of an impacted member, six slightly downscaled vehicle impact tests (2:3) were performed at RWTH Aachen University. Three different support conditions for the column were examined, including a simply supported column (ideally pinned) with and without a concentrated mass attached to the column head as well as a column with realistic boundary conditions and connections at column base and column head. By varying the boundary conditions and attached mass the influence of various types of interaction between the column and the surrounding structure was assessed experimentally. For the columns a HEB 140 steel section was selected; the nominal yield strength of the material was 355 MPa (coupon tests indicated 6% overstrength). Also the velocity of the impact body varied to achieve different degrees of impairment and residual strengths of the column. Table 1 summarizes the test program and the varied parameters.

For testing, the columns were arranged horizontally in front of a retaining wall with the strong axis of the steel section orthogonal to the impact direction. The dimensions of the column and the distance of the point of impact to the column base were selected within the limitations of the testing facility and can be found in Table 1. For test #2-1 & #2-2 a seven ton mass was connected to the pin joint at the column head. For test #3-1 & #3-2 the total length of the column was increased to 3.0 m with a realistic column to beam connection at a 'height' of 2.5 m and

Table 1: Overview of the test program.

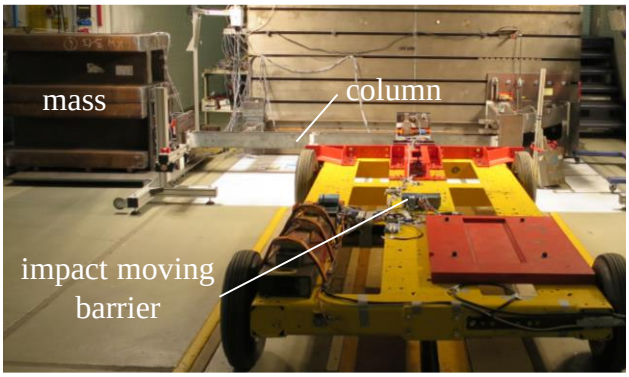

Figure 1: Photo of test setup for impact test 3-1/2.

the mass rigidly connected at 3.0 m (see Figure 1). In all tests the mass was supported by round steel bars to allow for free movement in axial direction of the column.

As an impactor, a very stiff impact moving barrier was used which was adjusted to a weight m_0 of 1500 kg. For the impact tests it was accelerated to a final impact velocity v_0 of 8 resp. 10 m/s. The kinetic energy stored in the impact vehicle at the time of the impact amounted to 48 or 75 kJ, respectively. The kinetic energy can be calculated with the well-known formula:

$$E_{kin,veh} = 0.5 \cdot m_0 \cdot {v_0}^2 \quad (1)$$

A block of aluminium honeycombs was mounted in front of the impact moving barrier to account for an idealized elasto-plastic force-displacement behaviour, which corresponds to the crashworthiness of a standard passenger vehicle. The plastic strength of the crush-area was determined to 300 kN under loading in axial direction by preliminary tests. With a crushable length of 320 mm, a total plastic energy of around 96 kJ could be absorbed by one honeycomb block. A steel plate was placed in front of the block to cater for a uniform load distribution in the honeycombs.

The columns were equipped with strain gauges in three different beam sections. Additionally optical marks were glued along the beam axis to allow for the extraction of displacement information from video footage, which was captured with a high speed camera (2000 fps). Acceleration sensors were placed at the point of impact on the column, at the centre of gravity of the impact vehicle and at the head mass. Draw wire sensors were connected to the supporting structure and to the head mass to track displacements of the supports and of the head mass. Force transducers were used to measure the force between the block of honeycombs and the impact vehicle (which corresponds to the contact force at the impacted section). For tests #2-1/2 and #3-1/2, additional force transducers were deployed to gauge the forces transferred between the head mass and the column head. Results of the experimental tests are presented together with the outcome of the numerical recalculations in chapter 3.2.

3 NUMERICAL RECALCULATIONS

Detailed Finite-Element models were deployed to perform numerical verification of the impact tests described in Section 2. For this purpose, the software LS-Dyna was used which is a powerful and proven tool for highly nonlinear problems in the short-term dynamic regime.

3.1 Model description

For the modelling of the steel column, endplates and the beam, connected to the column in test #3-1 and #3-2, shell elements (Belytschko-Tsay formulation) with a linear shape function and 5 integration points through shell thickness were used. Belytschenko-Wong-Chiang warping stiffness was added to increase the accuracy of the elements. The shells were discretised with a quadrilateral mesh, with an average element edge length of 10 mm. The impact moving barrier, including the block of honeycombs and the steel plate, used for load introduction, were modelled with hexahedral solid elements (single point integration formulation, type 1). Element edge lengths of 10 to 25 mm were applied for the deformable parts. In preliminary studies, a

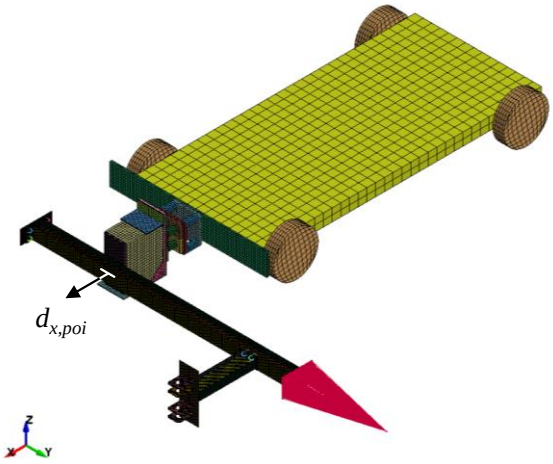

Figure 2: Model for recalculation of test 3-1/2

finer discretisation did not increase the quality of the results significantly. Proper hourglass control settings were applied for each element type to minimize the impact of zero energy hourglass modes.

An isotropic, multilinear material law was used to describe the stress-strain relationship of the S355 mild steel. The multilinear curve was adjusted to fit to the stress-strain curve obtained from tensile tests on the base material. LS-Dyna offers two material models for the description of honeycomb material which were investigated in preliminary studies. Although recommended element formulations and hourglass control preferences were set, the usage of Mat_126_MODIFIED_HONEYCOMB resulted in an emergence of significant hourglass energy in the honeycomb block (50% of the internal energy stored in the honeycomb after impact). Mat_26_HONEYCOMB was found to give much better results in this respect (with hourglass energies around 5% of the internal energy). The axial behaviour of the honeycomb was determined in static and dynamic (droptower) compression tests at RWTH Aachen and could be described as a bilinear function until fully compressed (at a total compression of 80%). However, the behaviour under off-axis loading was not assessed experimentally. Instead, assumptions for off-axis behaviour of the honeycombs have been met, based on current literature, e.g. [2]. All other parts of the impact moving barrier were modelled as non-deformable (rigid) bodies.

The hinges as well as the connection of the head mass were idealised as nodal rigid bodies with certain boundary conditions at their centre of gravity. To capture the effects of the impact load on the bolted, semi-strength connection, used in the experimental tests #3-1/2, a more detailed, realistic approach was followed. The shank of each bolt was modelled as an elastic spotweld beam and connected to circular shell plates at both ends, which represent the bolt head and the nut. Contact between the bolt shank and the bolt hole was established with the use of several elastic springs that behave very stiff under compression and soft in tension. An initial axial force was applied to the spotweld beams whereby the connected plates were compressed between the bolt head and the nut. The preload in the bolts and gravity load was initialised in a separate dynamic relaxation phase before the impact phase.

3.2 Results

Within this paper, selected examples of results are shown and discussed for brevity. The contact forces between the impact moving barrier and the column as well as the lateral displacements of the column at the point of impact are shown in Figure 3. Results of the experimental tests are represented as solid lines, whereby the numerical results are plotted in dashed lines. In the first phase of the impact, the contact force oscillates at an almost constant level. It can be observed, that the peak contact force varies only slightly in all tests, despite the differences in the test configurations (it is always limited by the plastic resistance of the honeycombs or the impacted column). However, there is a big difference in the column displacement at the point of impact. As can be expected, the simple supported setup without head mass and an impact speed of 10 m/s shows the highest deflections (300 mm plastic deformation) while the setup with the semi-strength connections and the connected head mass undergoes the lowest deflections (50 mm permanent deformation). The measured deflections in Test #2-1 and #2-2, which

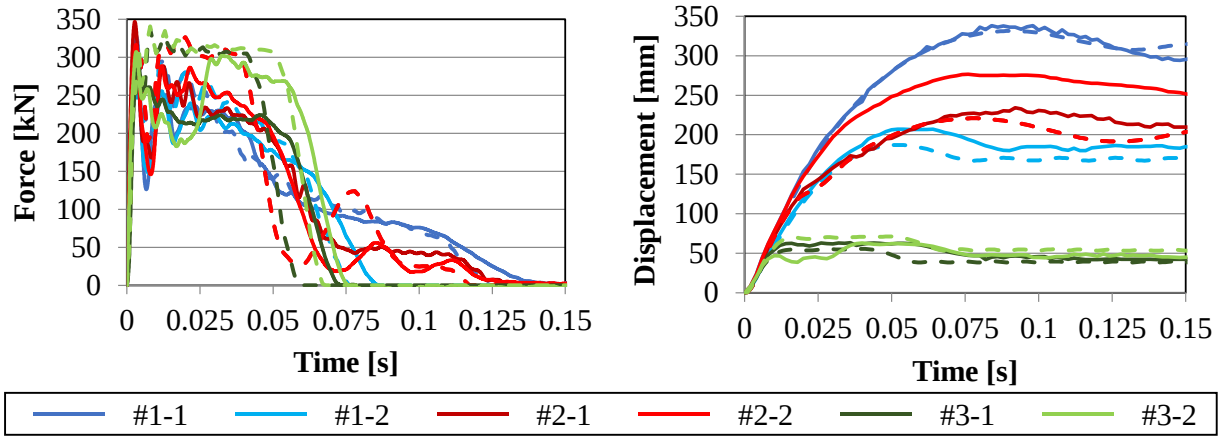

Figure 3: Contact Force between column and IMB (left), column displacement at the point of impact (right)

basically had identical test parameters (simply supported; with head mass; same impact velocity) differ significantly from each other (25% lower deflections at test #2-1 compared to #2-2). In both tests not negligible deformations of the support structure were observed, which could be the reason for the notable difference.

The energy stored in the column can be determined by integrating the force-displacement data shown in Figure 3.

$$E_{int,col} = \int F_{x,poi} \cdot dd_{x,poi} \tag{2}$$

Furthermore, the deformation energy of the aluminium honeycombs can be evaluated by integrating the force over the relative displacement between the impact moving barrier and the displacement of the column at the point of impact.

$$E_{int,veh} = \int F_{x,poi} \cdot d(d_{x,veh} - d_{x,poi}) \tag{3}$$

Finally, the kinetic energy of the impact moving barrier and the head mass, considered in test #2-1/2 and #3-1/2, can be calculated as a function of their velocity (adopting equation (3)). The total energy is obtained by summing up the separate values. The energetic (re-)distribution during the tests is shown in Figure 4.

Although the energy balance is not perfectly constant (e.g. friction work is neglected) it can be stated, that all relevant work portions are considered. The maximum deviation between input and output energy (10%) can be noticed in test #2-1. During this test, the head mass moved more than 60 mm in axial direction and strongly oscillated after the impact. Additionally, parts of the supporting structure slipped at the retaining wall. This resulted in additional energy dissipation through friction, which is not accounted for in the energy balance.

The kinetic energy is converted mainly into deformation energy in the steel member and the block of aluminium honeycombs. Since the plastic resistance of the honeycombs is slightly higher than the load that causes the formation of a plastic hinge in the simply supported case but lower than the one that is needed to initiate yielding in the realistically supported member, the ratio of the energy stored in the column and the energy in the aluminium honeycombs differs strongly from one test setup to another. This fits to the finding that the contact force seems to be roughly the same for all test setups, although the lateral displacements of the column at the point of impact differ significantly. The kinetic work, done by the head could not be calculated for test #2-1, since no acceleration signal was measured during that test.

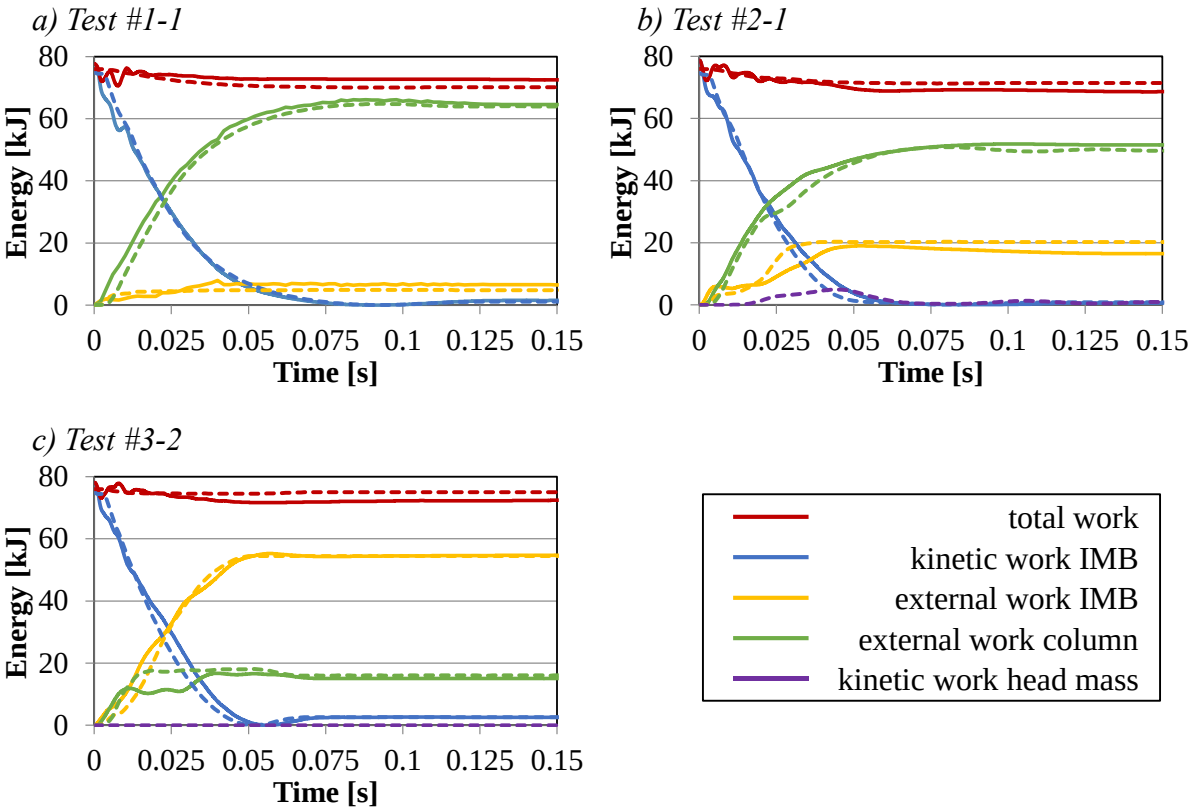

Figure 4: Energy (re-)distribution during tests with different setups.

4 PARAMETRIC STUDY

In addition to the numerical recalculations, a parametric study was performed to further investigate the influence of relevant parameters on the dynamic response of an impacted steel column. As for the numerical recalculations, LS-Dyna was used as a simulation tool. Material parameters, modelling techniques and control settings that proved successful for the recalculation were adopted for the parametric study as well.

4.1 Model description

For the parametric study, a HEB 220 column with a height of 3.6 meters was modelled using shell elements. All nodes at the column base and column head were coupled and the boundary conditions were applied to the master node in the centre of gravity of the section. Discrete spring elements were used to account for partially stiff joint rotation behaviour at the column base and the column head. The head mass was described as a discrete translational point mass and was rigidly connected to the column head.
The impactor was simplified as a solid block with a height of 0.25 meters and a width greater than the width of the impacted column. The weight of the impacting body was adjusted to 1.5 tons. For the parametric study, the impactor was considered to behave very stiff and purely elastic which implicates that the kinetic energy stored in the impactor is completely transformed into strain work in the impacted column and not in the impactor. This allows for better comparison of the column response at a certain level of kinetic energy input into the system. In all tests the point of impact was chosen to 0.625 m above the column base. The general model for the

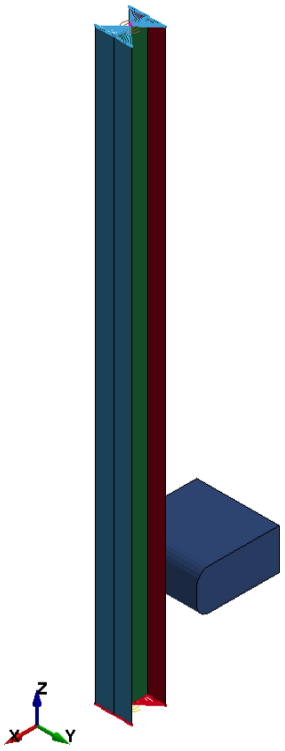

Figure 5: Model for the parametric study.

parametric study is shown in Figure 5. For the study the following parameters have been selected for further investigation:

- Boundary conditions at the column base and column head to represent different joint configurations
- Mass and weight of the head mass to account for various utilization levels of the column by gravity loads
- Impact velocity to simulate different impact scenarios

More than 40 simulations have been performed and evaluated. The most important findings are discussed within the next section.

4.2 Results

The two diagrams in Figure 6 show the maximum lateral deflection of columns with different rotational boundary conditions at the point of impact. Three different rotational stiffness variations – 0 kNm/rad (pinned support), 10.000 kNm/rad and ∞ kNm/rad (rigid support) – have been applied. Furthermore, the weight of the head mass varied from 0 to 200 tons. For comparison, a fully axially restraint column (res) was also included in the numerical study. The results shown in the left diagram correspond to an impact velocity of 60 km/h whereas the lateral deformations shown in the right diagram were obtained with an impact velocity of 80 km/h. The red columns indicate a collapse of the impacted member due to global buckling accompanied by local bucking of the web at the point of impact. The maximum lateral displacements, obtained at the end of the simulations with column collapse are higher than 350 mm in most cases but trimmed in the diagrams to allow for a better visibility of other values.

By comparing the maximum lateral deflections of the impacted column, several conclusions can be drawn. Not surprisingly, the boundary conditions have a significant influence on the deformation behaviour of the impacted column. The lateral deformations in the column decrease with increasing rotational stiffness at the column base and the column head. The rotational stiffness at the column base has a higher influence on the global stiffness of the impacted system than the rotational stiffness at the column head resulting from higher rotational demands. The hinged columns without axial restraint suffer severe local deformations and buckling of the web at the height of impact which results in a noticeably reduced axial load bearing capacity and a subsequent collapse of the column. The systems with a rotational stiffness of 10000 kNm/rad at the column base and column head ($v_0 = 80$ *km/h*) yield almost identical results compared to the rigidly connected system with the same impact velocity.

Obviously, different impact velocities lead to different degrees of lateral deformation in the column. The higher the impact velocity, the higher the lateral displacements for a given system configuration as can be recognized comparing both diagrams shown in Figure 6. In average, the lateral deflection increase by 50% due to the higher impact velocity. This is considerably less than one could expect following simplified energy based approaches to determine the lateral deflection (e.g. [3] or [4]). Here the lateral deflections are more or less proportional to the kinetic energy of the impactor which increases with the square of the impact velocity. However, these approaches assume an idealized plastic mechanism neglecting local distortions at the point

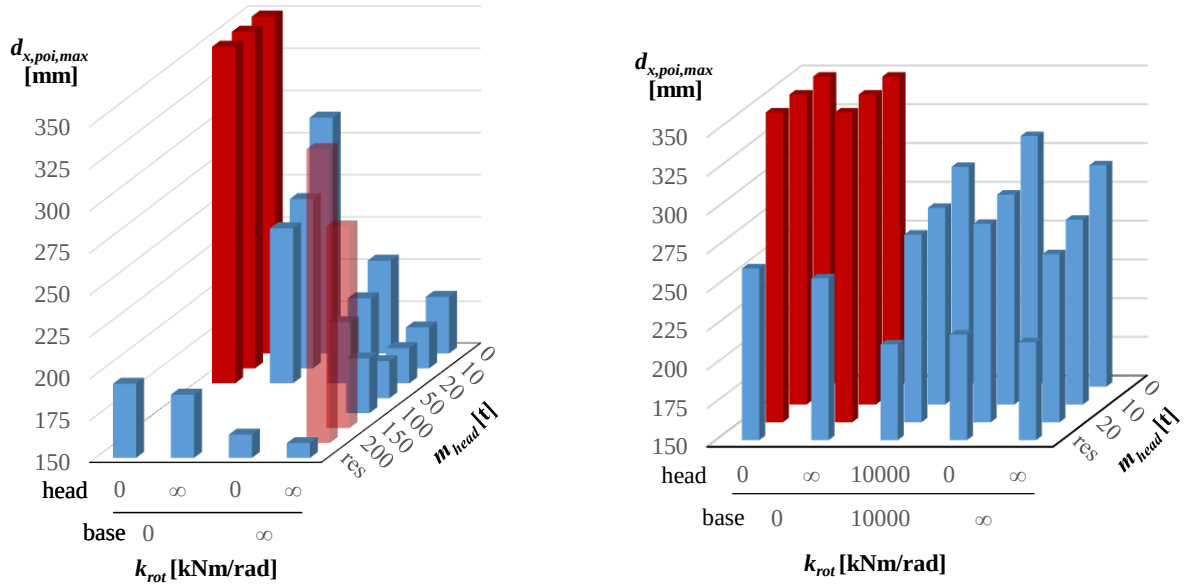

Figure 6: Maximum lateral deflections of the column at the point of impact.
(m_0=1.5 t, v_0=60 km/h (left), v_0=80 km/h (right))

of impact as well as the effect of an attached head mass. Moreover, strain rate and strain hardening effects are mostly disregarded in these simplified approaches.

Considering the influence of the head mass two opposite effects can be observed on the maximum lateral displacement at the point of impact. In the first phase of the impact, the inertia of the head mass adds a short term axial restraint to the system. In consequence, considerable axial tensile forces develop in the column. In the second phase of the impact, the head mass accelerates and starts moving towards the column base. This causes the development of dynamic compression forces which can lead to further plastification in the impacted zone or in combination with the gravity load to complete collapse of the column due to P-Δ effects. As can be seen in Figure 6 even small head masses provide enough inertia to generate an initial axial restraint resulting in decreasing maximum lateral displacements at the point of impact. However for heavier head masses the resulting maximum lateral displacements can increase until collapse due to the latter effect.

Figure 7 shows axial forces at the top of the column as well as the lateral deflections at the point of impact for the column configuration with infinite rotational stiffness and different head masses at an impact speed of 60 km/h (which corresponds to the results shown on the rightmost row of the left diagram in Figure 6). At time $t = 0$, the gravity load acts on the column resulting from the head mass and the initial lateral deflections at the point of impact are zero. During the impact, the lateral deflections at the point of impact rapidly increase. As described before, noticeable tensile forces develop at the column head, since the shortening of the column is impeded by the inertia of the head mass. Subsequently, the head mass accelerates and pushes at the column head. The compressive forces reach maximum values of 2200-2300 kN and cause further deformations in the plastic hinge at the point of impact. In case the deflected column has sufficient resistance to withstand and to absorb the compressive impulse, the axial force in the column oscillates around the static force value until the head mass comes to rest (0-100 tons). For the head masses with a weight 150 and 200 tons, a complete collapse of the column can be observed. Further investigations have been performed to study the collapse mechanism in these cases.

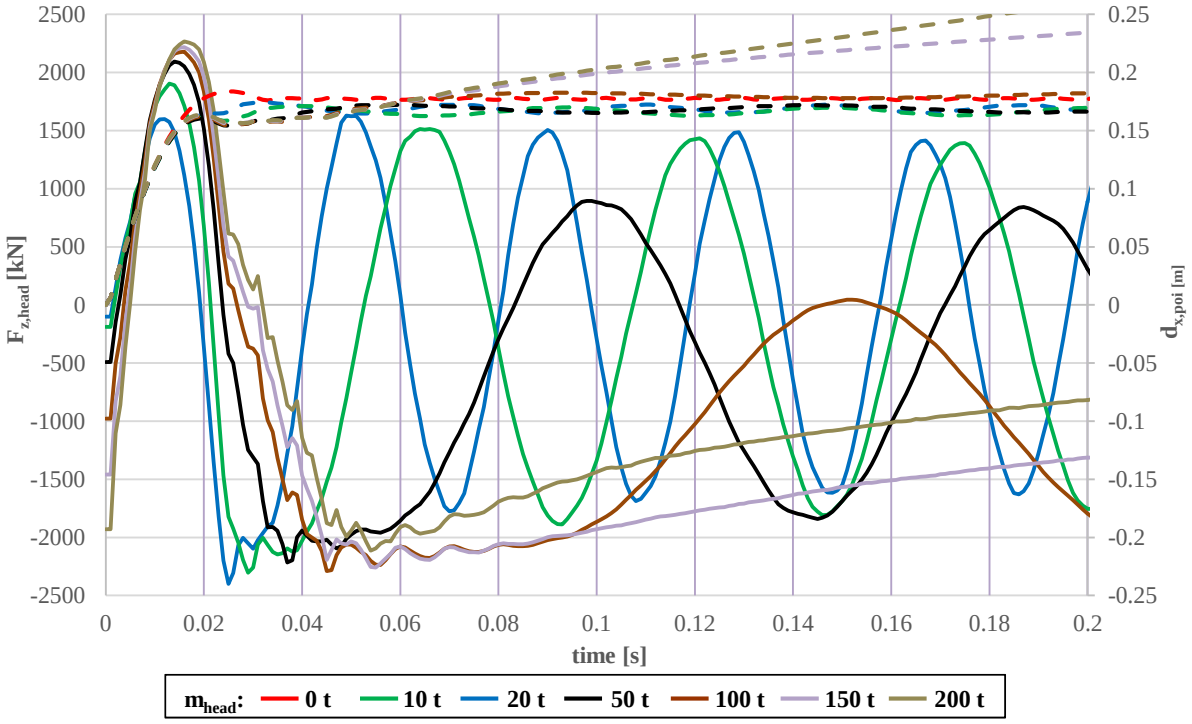

Figure 7: Axial Forces (solid lines) at the column head and lateral displacements (dashed lines) at the point of impact over time. (m_0 = 1.5 t, v_0 = 60 km/h, $k_{rot,base} = k_{rot,head} = \infty$)

In a first step, the chronology of the collapse progress is assessed. Based on the history of contact forces at the point of impact and axial forces at the column head it can be assumed that the impact event and the subsequent increase in lateral deflections caused by the head mass can be considered as two separate events. Thus, the compression of the column caused by the accelerated head mass can be described as a secondary impact at the column head in axial direction. However, the lateral deformation of the column resulting from the initial, lateral impact event must be incorporated. In contrast to the simply supported systems that collapse (see Figure 6) no significant local deformations can be noticed for the clamped columns ($k_{rot,base} = k_{rot,head} = \infty$) as a consequence of the initial, lateral impact.

A common approach to assess the axial residual strength of the deformed system is to perform a pushover analysis applying an increasing axial load at the head of the pre-damaged column. Under quasi static load conditions the column could be considered beyond its ultimate limit state if the maximum force, resulting from the pushover analysis is lower than the static gravity load of the head mass. However the calculated dynamic axial forces significantly exceed the static gravity forces as can be seen in Figure 7. As a consequence the dynamic load component of the head mass can't be neglected in this contemplation.

To account for the dynamic component of the head mass, an energy based approach is proposed. If the static gravity load is below the maximum force resulting from the pushover analysis it can be taken as an offset for the calculation of the residual external work that the column can absorb until it collapses. Additional energy input (e.g. in the form of kinetic energy of the head mass) leads to increasing elastic or plastic deformations in the column. The maximum residual work that can be done until collapse corresponds to the area under the pushover curve with a lower limit given by the quasi-static gravity load ($F_{z,head,qs}$).

$$E_{int,col,res} = \int \left(F_{z,head} - F_{z,head,qs}\right) \cdot du_{z,head} \qquad \text{for } F_{z,head} > F_{z,head,qs} \qquad (4)$$

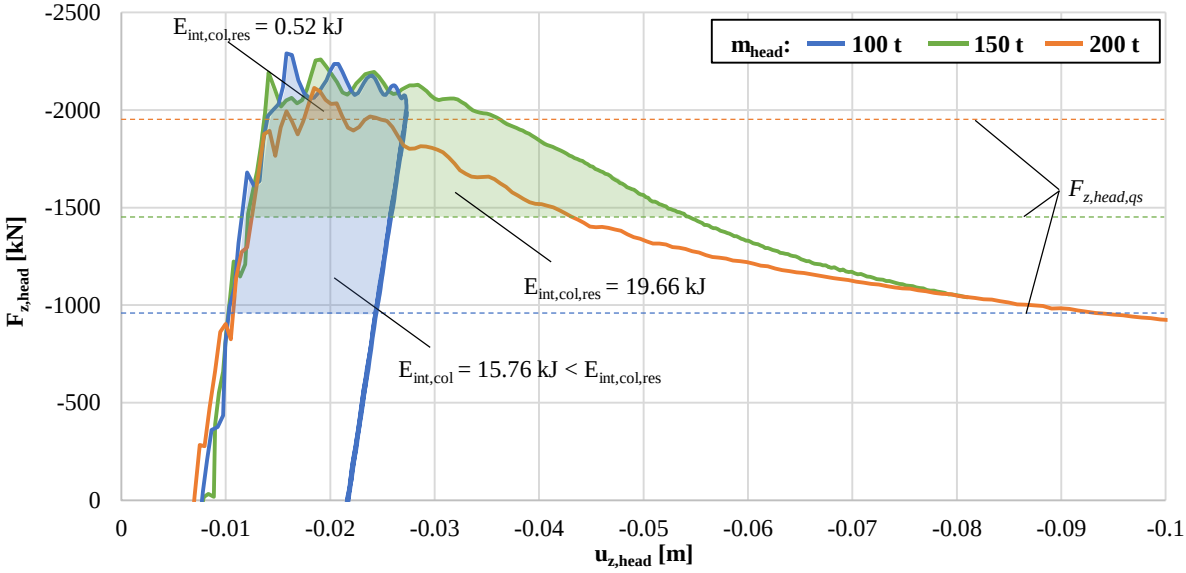

Figure 8: Axial compressive forces at the column head and corresponding axial displacements.
(m_0 = 1.5 t, v_0 = 60 km/h, $k_{rot,base}$ = $k_{rot,head}$ = ∞)

If the kinetic energy of the accelerated head mass is higher than the residual external work, the column fails. This assumption can be assessed by reviewing Figure 8. Here, the compressive axial forces are plotted dependent on the axial displacement at the column head (shortening of the column) for selected setups. The highlighted areas under the curves correspond to the kinetic energy of the head mass that is transformed into strain energy in the column as a result of the secondary impact. The two curves for the setups with 150 (green) and 200 (orange) tons head mass can be seen as pushover curves, since the impact of the accelerated head mass causes a complete collapse of the column. In these cases the kinetic energy which amounts to 21.7 kJ for the 150 ton head mass and 28.8 kJ for the 200 ton head mass exceed the respective residual capacity of the deformed column. The blue curve corresponds to the setup with 100 tons head mass which does not collapse. Here the blue area is equal to the kinetic energy that is converted into plastic strain energy in the column. The maximum kinetic energy of the head mass before the first compressive cycle amounts to 17.69 kJ and decreases to 2 kJ in subsequent oscillation cycles. The difference between the kinetic energy before and after the first compressive cycle is almost equal to 15.76 kJ which corroborates the assumptions made before. The remaining energy of 2 kJ is shifting its form from kinetic energy to elastic strain energy in the column in each cycle.

5 SUMMARY AND CONCLUSIONS DRAWN

The work presented within this paper covers the description of full scale impact tests performed at the University of Aachen. In addition, numerical recalculations have been performed using refined LS-Dyna models. Subsequent to the calibration of the finite element models, numerical investigations have been extended to a parametric study on isolated columns under impact loading to assess the influence of different boundary conditions, the weight of the connected head mass as well as varying impact velocities.

The impact tests were conducted with an impactor with elastic, perfectly plastic behaviour. Depending on the boundary conditions of the impacted column, different shares of the input energy were transformed into plastic strain energy in the column and the impacting vehicle. If no head mass was considered, the energy redistribution was found to mostly depend on the plastic capacity of the impact vehicle and the impacted member. By adding a head mass to the

column head, the lateral displacements at the point of impact were reduced noticeably in the test.

These observations were confirmed in the numerical simulations. However, when gravity loading was considered, the head mass imposed additional lateral displacements in a *secondary* impact event. While already small head masses provided a certain axial restraint and in fact decreased the lateral deflections during vehicle impact, heavier head masses led to increasing total lateral deflections as a result of the aforementioned *secondary* impact. In this respect it is important to notice that the impacted member must not only be able to carry the static component of the head mass (gravity load) but also needs to be able to absorb the kinetic energy imposed by the accelerated head mass without collapse.

The investigations on isolated columns, presented within this paper, will be complimented by impact simulations at the global structural level, considering the stiffness of the surrounding structure, realistic mass distribution and catenary effects of connected beams.

6 ACKNOWLEDGEMENT

The work presented here is carried out as a research project by different European partners with a financial grant from the Research Fund for Coal and Steel (RFCS) of the European Community. The authors gratefully acknowledge the financial support.

REFERENCES

[1] HAUKE B. et al., "Composite Column and Wall System for Impact and Blast Resistance – Final report RFS-CR-04047", RFCS publications, European Commission, Brussels, 2008

[2] JACKSON K. et al., "Material Model Evaluation of a Composite Honeycomb Energy Absorber", Proceedings of the 12th international LS-DYNA Users Conference, Detroit, June 3-5, 2012

[3] M. Gündel, B. Hoffmeister und B. Hauke, „Bemessung von Baustrukturen in Stahl- und Verbundbauweise für Anprall- und Explosionslasten", >>bauforumstahl e.V., Düsseldorf, 2010.

[4] N-004: Norsok Standard: Design of steel structures, 2004.